JACS
JOURNAL OF THE AMERICAN CHEMICAL SOCIETY
Article
pubs.acs.org/JACS

Nanoparticle Size and Surface Chemistry Determine Serum Protein Adsorption and Macrophage Uptake

Carl D. Walkey,[†,§] Jonathan B. Olsen,[‡,§] Hongbo Guo,[‡,§] Andrew Emili,[‡,§] and Warren C. W. Chan*[,†,§,⊥,∥,#]

[†]Institute of Biomaterials and Biomedical Engineering, [‡]Banting and Best Department of Medical Research, [§]Donnelly Centre for Cellular and Biomolecular Research, [⊥]Department of Chemical Engineering, [∥]Department of Chemistry, and [#]Department of Materials Science and Engineering, University of Toronto, Toronto, Ontario, Canada M5S 3G9

Supporting Information

ABSTRACT: Delivery and toxicity are critical issues facing nanomedicine research. Currently, there is limited understanding and connection between the physicochemical properties of a nanomaterial and its interactions with a physiological system. As a result, it remains unclear how to optimally synthesize and chemically modify nanomaterials for *in vivo* applications. It has been suggested that the physicochemical properties of a nanomaterial after synthesis, known as its "synthetic identity", are not what a cell encounters *in vivo*. Adsorption of blood components and interactions with phagocytes can modify the size, aggregation state, and interfacial composition of a nanomaterial, giving it a distinct "biological identity". Here, we investigate the role of size and surface chemistry in mediating serum protein adsorption to gold nanoparticles and their subsequent uptake by macrophages. Using label-free liquid chromatography tandem mass spectrometry, we find that over 70 different serum proteins are heterogeneously adsorbed to the surface of gold nanoparticles. The relative density of each of these adsorbed proteins depends on nanoparticle size and poly(ethylene glycol) grafting density. Variations in serum protein adsorption correlate with differences in the mechanism and efficiency of nanoparticle uptake by a macrophage cell line. Macrophages contribute to the poor efficiency of nanomaterial delivery into diseased tissues, redistribution of nanomaterials within the body, and potential toxicity. This study establishes principles for the rational design of clinically useful nanomaterials.

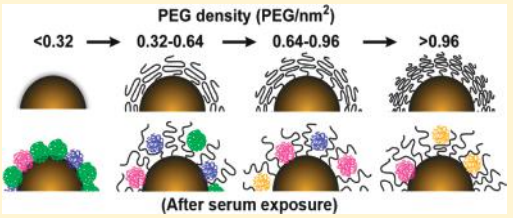

INTRODUCTION

By virtue of their unique physical and structural properties, engineered nanomaterials have the potential to dramatically improve the treatment and diagnosis of disease.[1−6] However, the inability to control their pharmacokinetics and biodistribution has hindered widespread realization of this potential.[7−9] Most nanomaterial formulations are rapidly sequestered by cells of the mononuclear phagocyte system (MPS) following intravenous administration.[10−12] The MPS consists of dendritic cells, blood monocytes, and tissue-resident macrophages in the liver, spleen, and lymph nodes that are responsible for clearing, processing, and degrading foreign materials from circulation.[13] On top of lowering the dose available for accumulation at a therapeutic site, MPS uptake can lead to inflammation,[14] compromised host defense,[15] release of toxic byproducts,[16] and redistribution of nanomaterials to sensitive areas in the body.[17] Moreover, uncertainty regarding the eventual fate of nanomaterials after they accumulate in MPS organs raises the possibility of delayed or chronic toxicity.[18] Uncontrolled and often unpredictable localization, along with concerns regarding toxicity, have created a barrier to the clinical translation of many engineered nanomaterials.[19] Tailoring the interaction of nanomaterials with physiological systems has become a focus of nanomedicine research.

Physiological environments, such as blood, interstitial fluid, and cellular cytoplasm, contain complex mixtures of proteins. When a nanomaterial enters a physiological environment, these proteins rapidly adsorb to its surface and form what is known as the protein "corona".[20] The protein corona alters the composition of the nanomaterial along with its aggregation state, giving it a "biological identity" that is distinct from its "synthetic identity"—the surface chemistry, size, and shape of a nanomaterial after synthesis.[21] The biological identity is the form of a nanomaterial "seen" by biomolecules, cells, and biological interfaces, and is responsible for the kinetics, transport, and reactivity of a nanomaterial in a physiological system.[22] Adsorption of blood proteins is most relevant and most studied since nanomaterials are typically administered intravenously. Blood contains thousands of different proteins, each of which may potentially interact with a nanomaterial.[23] The blood protein corona is complex, consisting of dozens of proteins including apolipoproteins, adhesion mediators, signaling and transport proteins, complement components, and coagulation factors.[21] Many of these proteins act as opsonins that mark a nanomaterial for efficient uptake by MPS phagocytes either in their native state[11] or after undergoing a conformational change.[24] In addition, adsorbed proteins can modulate the activation of enzymatic cascades, leading to thrombosis or anaphylaxis.[25] Recent studies have shown that

Received: September 12, 2011
Published: December 22, 2011

dx.doi.org/10.1021/ja2084338 | J. Am. Chem.Soc. 2012, 134, 2139−2147

the synthetic identity of a nanomaterial plays an important role in determining the composition of the protein corona and the subsequent cellular interactions.[26−29] However, relationships linking the size, shape, and surface chemistry of a nanomaterial to protein adsorption and phagocytic cell uptake are poorly developed.

The most widely applied strategy to block nonspecific protein adsorption and phagocyte uptake is to graft nanomaterials with linear chains of poly(ethylene glycol) (PEG)—a process known as "PEGylation".[30] PEG suppresses protein adsorption by blocking protein-binding sites and by creating a thermodynamic barrier to protein diffusion.[31−33] Grafting nanomaterials with PEG is effective at slowing the rate of MPS uptake and prolonging blood residence time.[34,35] Despite the wide application of PEG, it remains unclear how the design of PEGylated nanomaterials influences blood protein adsorption and subsequent phagocyte uptake.[36] This has led to varying performance between formulations with some achieving blood half-lives in excess of 24 h, while others have half-lives measured in minutes.[8,10,37,38] Here, we use a gold nanoparticle model system to investigate the effect of size and PEG grafting density on serum protein adsorption and macrophage uptake. By understanding the influence of these key design parameters, this study establishes principles for the rational design of PEGylated nanoparticles with controlled protein adsorption and effective phagocyte evasion.

RESULTS AND DISCUSSION

We synthesized 15, 30, 60, and 90 nm gold nanoparticles using established techniques[39] and grafted them with thiolated, methoxy-terminated PEG at densities ranging from 0 (ungrafted) to 1.25 PEG/nm^2. We chose to study a single PEG molecular weight of 5 kDa since protein adsorption is predominantly a function of PEG grafting density above a molecular weight of ∼1 kDa.[33,40] Grafting density was controlled by varying the PEG-to-nanoparticle grafting stoichiometry, and quantified by a thiol depletion assay (Figure S1a). In all cases, PEG grafting density was below the measured size-dependent saturating density (Figure S1b).

The maximum PEG grafting densities achieved in this study are considerably higher than those typically reported for "flat" substrates.[40−43] We credit this to the highly curved surface of the nanoparticles, which limits PEG−PEG steric interactions, along with an elevated grafting temperature (60 °C), which leads to partial dehydration of PEG molecules.[44] Both of these factors permit more PEG molecules to pack onto the nanoparticle surface during grafting, raising the maximum grafting density. The small footprint of thiols coordinated to gold (∼0.17 nm^2) means that the maximum grafting density is limited by PEG−PEG steric interactions, not saturation of available tethering sites.[45]

After synthesis, we measured the size, morphology, hydrodynamic diameter, and polydispersity of our nanoparticles using transmission electron microscopy (TEM) and dynamic light scattering (DLS) to verify that they are monodisperse, stable, and uniformly grafted with PEG (Figures S2 and S3). Combining these measurements allowed us to estimate the hydrodynamic volume occupied by each PEG molecule (V_{PEG}) on the nanoparticle surface (Figure 1a,b). As PEG grafting density increases, compression of neighboring PEG molecules decreases V_{PEG} nonlinearly. A smaller V_{PEG} implies that the grafted PEG molecules lose conformational freedom and dehydrate, increasing the thermodynamic barrier to protein

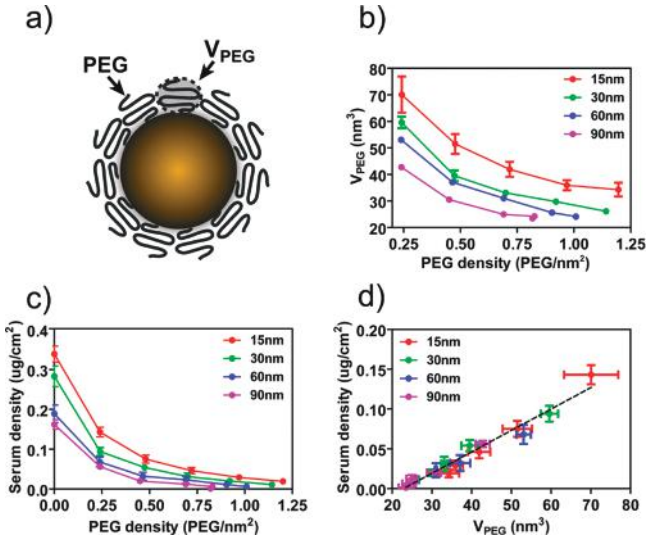

Figure 1. Size and poly(ethylene glycol) (PEG) grafting density determine PEG conformation and total serum protein adsorption to gold nanoparticles. (a) Diagram illustrating PEG molecules tethered to a gold nanoparticle. The average PEG hydrodynamic volume (V_{PEG}) is indicated. (b) V_{PEG} as a function of PEG grafting density. V_{PEG} was measured by dividing the difference in hydrodynamic volume of gold nanoparticles before and after PEG grafting by the number of PEG molecules per nanoparticle. Under equal PEG density, the curved surface of smaller nanoparticles permits a larger V_{PEG} by decreasing steric interactions between neighboring PEG molecules. (c) PEG grafting density determines total adsorbed serum protein density. PEG-grafted gold nanoparticles were incubated in human serum and washed to remove unbound protein. Adsorbed protein density was measured by the bicinchoninic acid (BCA) assay. Adsorbed serum protein density was statistically significant at all PEG densities tested ($p < 0.05$). (d) When expressed as a function of V_{PEG}, nanoparticle size does not influence adsorbed serum protein density, suggesting that size-dependent differences in total protein adsorption are the result of curvature-dependent differences in PEG−PEG steric interactions. Linear regression was performed by minimization of the sum of squares. All data points are mean ± SEM of 3−5 independent replicates.

diffusion within the PEG chains and adsorption to the nanoparticle surface.[31,40,46] With equal grafting density, V_{PEG} is larger on smaller nanoparticles since increased surface curvature reduces steric interactions between neighboring PEG molecules. Analogous observations have been made for other macromolecules such as DNA.[47] These results demonstrate that a combination of nanoparticle size and PEG density determine the conformational freedom of grafted PEG molecules, along with the thermodynamic barrier to protein adsorption.

To directly study the effect of nanoparticle size and PEG grafting density on serum protein adsorption, we incubated PEG-grafted gold nanoparticles in human serum and measured total protein adsorption by the bicinchoninic (BCA) assay (Figure 1c). Ungrafted nanoparticles adsorbed a dense layer of protein, confirming that the unmodified gold surface interacts strongly with serum proteins.[48] For a fixed nanoparticle size, increasing PEG grafting density reduces total protein adsorption nonlinearly. At the highest PEG densities tested, 94−99% of serum protein adsorption was eliminated relative to ungrafted nanoparticles, but remained statistically significant. Further increases in PEG grafting density may further reduce

dx.doi.org/10.1021/ja2084338 | J. Am. Chem.Soc. 2012, 134, 2139−2147

serum protein adsorption, provided direct adsorption to the grafted PEG molecules does not occur.[40]

Under fixed PEG grafting density, decreasing nanoparticle size increases total protein adsorption. However, when expressed as a function of V_{PEG} (instead of PEG density), total protein adsorption is independent of nanoparticle size (Figure 1d). This suggests that size-dependent differences in protein adsorption are the result of curvature-dependent differences in PEG−PEG steric interactions. In other words, PEG molecules have more room to "spread-out" on the highly curved surface of small nanoparticles, which lowers the thermodynamic barrier to protein adsorption. This finding is in contrast to the widely held view that decreased PEG chain conformational freedom on larger nanoparticles will enhance, not suppress, protein adsorption.[30]

We observed a monotonic decrease in total protein adsorption with increasing PEG density, rather than an initial decrease followed by an increase that was observed in several studies using purified proteins adsorbed to "flat" substrates.[40,41] In those studies, it was hypothesized that the combined action of multiple PEG distal terminal groups could support protein adsorption to the PEG layer at high grafting density.[40] These "distal effects" were observed *in situ* for grafted PEG layers with methoxy but not hydroxyl distal terminal groups. In our study, we performed multiple washing steps to remove unbound serum proteins prior to measuring total protein adsorption. The washing procedure may have stripped weakly adsorbed proteins from the outer PEG layer, accounting for the disparity in the observed trend. In addition, the lower effective density of distal terminal groups on the curved nanoparticle surface may contribute.

Next, we examined the molecular composition of the adsorbed serum protein layer using polyacrylamide gel electrophoresis (PAGE) coupled with a fluorescent protein stain. Protein isolates from ungrafted nanoparticles showed complex band patterns, indicating that the adsorbed serum protein layer consists of a number of different proteins spanning a range of densities (Figure 2). Increases in PEG density decreased net lane intensity, consistent with the results from the BCA assay. However, even at high PEG grafting densities, faint bands between 50 and 80 kDa are apparent in the sample lanes. These bands were not present in the control lane, confirming that protein adsorption to the gold nanoparticles was not fully eliminated even at high PEG grafting densities. On top of decreasing total protein adsorption, increasing PEG density also changed the intensity of each band relative to the total for that lane (Figure S4). This implies that the composition of the adsorbed protein layer is a function of PEG density. To gain a more in-depth understanding of this phenomenon, we digested adsorbed protein isolates with trypsin and analyzed the resulting peptide mixtures by label-free liquid chromatography tandem mass spectrometry (LC-MS/MS).[49] LC-MS/MS enables simultaneous identification and relative quantification of proteins in a complex mixture with high reproducibility and sensitivity (Figure S5).[50] A total of 147 serum proteins of varying molecular weight, structure, and physiological function were identified, with relative abundances spanning over 3 orders of magnitude (Table S3). Adsorbed proteins with abundances of at least 0.25% w/w (70 total) are summarized in a heat map (Figure 3). Examining the rows of the heat map shows that the relative density of each adsorbed protein varies with PEG density. For example, complement factor C3 (CO3) constitutes over 30% w/w of

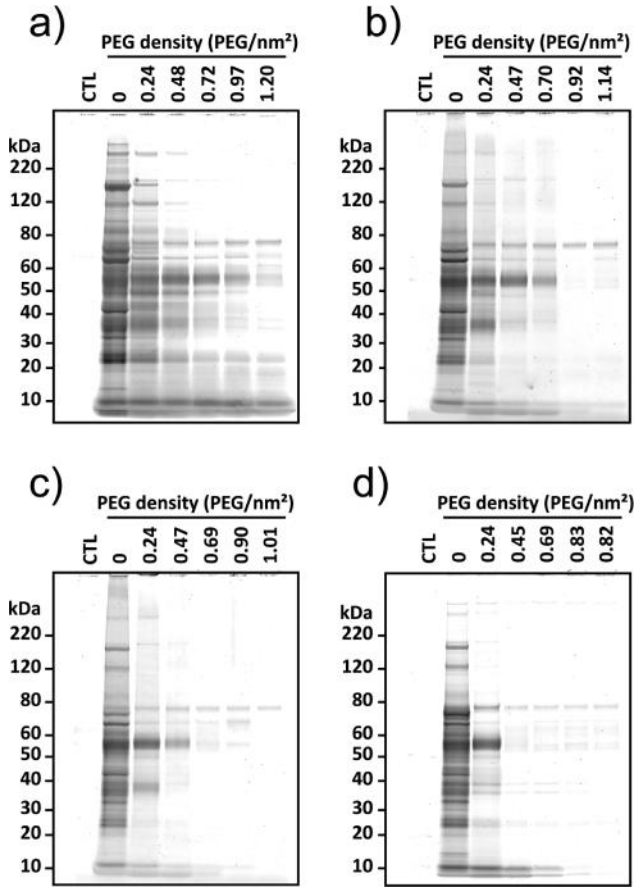

Figure 2. Qualitative molecular composition of the adsorbed serum protein layer on (a) 15, (b) 30, (c) 60, and (d) 90 nm gold nanoparticles grafted with PEG at varying density. Protein isolates were resolved by polyacrylamide gel electrophoresis (PAGE) and visualized with a fluorescent total protein stain. Images were recorded using a laser scanner. "CTL" denotes background control consisting of serum without particles. Each lane represents protein isolates from an equal total nanoparticle surface area. Changes in net lane intensity reflect variations in total adsorbed protein density. The complexity of the band pattern in each lane reflects the complexity of the adsorbed serum protein layer. Densitometric analysis of the gels is reported in Figure S4.

total adsorbed protein on ungrafted nanoparticles, but less than 5% w/w on nanoparticles grafted with PEG at 1.12 PEG/nm^2. On the other hand, kininogen (KNG1) constitutes less than 2% w/w of total adsorbed protein on ungrafted nanoparticles, but over 13% w/w on particles grafted with PEG at 0.80 PEG/nm^2.

We used cluster analysis to divide the identified serum proteins into four groups based on the correlation in their relative abundances (Figure 3). Proteins in clusters A, B, C, and D adsorb preferentially to nanoparticles grafted with PEG at low (0−0.32 PEG/nm^2), low-intermediate (0.32−0.64 PEG/nm^2), intermediate-high (0.64−0.96 PEG/nm^2), and high (>0.96 PEG/nm^2) densities, respectively. Preferential adsorption is probably the result of differences in the structure and chemical composition of the proteins in each group that enhance their affinity to nanoparticles grafted with PEG at specific densities. Densitometric analysis of the PAGE gels in Figure 2 revealed a tendency for higher molecular weight proteins to be preferentially blocked at low PEG densities (Figure S4f). As a result, the adsorption of smaller proteins is favored as PEG density increases. It is known that proteins face

dx.doi.org/10.1021/ja2084338 | J. Am. Chem.Soc. 2012, 134, 2139−2147

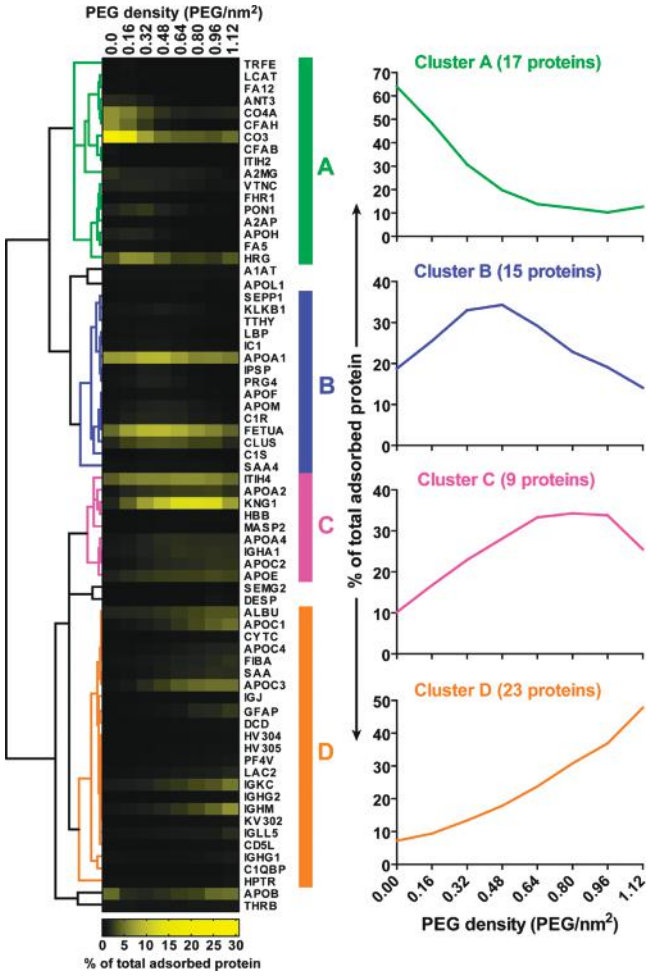

Figure 3. PEG density determines the composition of the adsorbed serum protein corona. Adsorbed serum proteins were isolated from 15 nm gold nanoparticles grafted with PEG at varying density, purified, digested with trypsin, and characterized by label-free liquid chromatography-tandem mass spectrometry (LC-MS/MS). A total of 147 proteins were identified. The 70 most abundant proteins are depicted in the heat map. Each row corresponds to a protein, and each column corresponds to a PEG density. Abbreviated protein names are explained in Table S3. The intensity of the yellow color is related to the abundance (by mass) of a given protein at a particular PEG density, based on the relative number of measured peptide spectra (spectral counts). Proteins were clustered into one of four groups: A, B, C, or D (represented by colored bars) based on correlation in their relative abundance across PEG densities. The dendrogram used to assign groups is shown on the left side of the heat map. The net relative abundance of each group (as a % of total adsorbed serum protein) is reported in the graphs to the right of the heat map, along with the number of proteins per cluster. Proteins from each cluster preferentially adsorb to nanoparticles grafted with PEG at low (cluster A), low-intermediate (cluster B), intermediate-high (cluster C), or high (cluster D) density. Reported quantities are the average of three independent replicates.

different thermodynamic barriers to penetration through the PEG layer, depending on their size, shape, and attraction to the nanomaterial surface.[31,51] Together, these results show that nanoparticle size and PEG grafting density control the composition of the adsorbed protein layer by selectively blocking or permitting the adsorption of specific proteins from serum.

Since PEG grafting density determines the quantity and identity of adsorbed serum protein, we hypothesized that it also determines the efficiency of macrophage uptake by regulating the interaction of nanoparticles with cell-surface receptors. We measured total uptake of PEG-grafted gold nanoparticles by J774A.1 murine macrophage-like cells using inductively coupled plasma atomic emission spectroscopy (ICP-AES). J774A.1 cells were selected as a model for MPS macrophages since they express many of the same cell-surface receptors responsible for pathogen clearance.[52] Ungrafted nanoparticles were taken up extensively after 4 h of cell exposure (Figure 4a). Below 0.5 PEG/nm^2, macrophage uptake is a function of PEG grafting density for all nanoparticle sizes. At ~0.5 PEG/nm^2, macrophage uptake was reduced by a factor of 20 to 169 relative to ungrafted nanoparticles (Figure S6). Further increases in PEG grafting density beyond 0.5 PEG/nm^2 did not have a measurable effect on net macrophage uptake, which remained statistically significant for all nanoparticle sizes (Figure 4a, inset). TEM analysis revealed that, regardless of PEG grafting density, nanoparticles are predominantly located within cytoplasmic vesicles, and are not adhered to the cell surface (Figures 4b and S7). Ungrafted nanoparticles were present in dense aggregated clusters inside vesicles, whereas particles grafted with PEG at 0.48 or 0.96 PEG/nm^2 were mostly dispersed and found at low frequency inside larger vesicles. We conclude that PEG grafting reduces macrophage uptake of nanoparticles in a size- and PEG density-dependent manner, but cannot completely eliminate it.

We noticed that increasing PEG density beyond ~0.5 PEG/nm^2 reduced serum protein adsorption to nanoparticles without altering macrophage uptake (Figure S8), suggesting that minimization of macrophage uptake does not require complete elimination of serum protein adsorption. To test this hypothesis, we measured J774A.1 uptake of PEG-grafted gold nanoparticles using serum-free culture after preincubating nanoparticles in either whole serum or serum albumin. This allowed us to resolve total macrophage uptake into serum-dependent and serum-independent components (Figure 4c). Below ~0.16 PEG/nm^2, macrophage uptake is almost completely serum-dependent. In contrast, above ~0.64 PEG/nm^2, over 90% of macrophage uptake is serum-independent, irrespective of nanoparticle size. In other words, serum proteins adsorbed to nanoparticles grafted with PEG above ~0.64 PEG/nm^2 are insignificant in the uptake process. This suggests that cluster A and B proteins (Figure 3) are most influential in mediating macrophage uptake, while proteins from clusters C and D are less important. Indeed, the most significant member of cluster A is complement component C3, which promotes clearance of pathogens, apoptotic cells, and particulates via interaction with macrophage complement receptors.[53,54] While C3 adsorbed at high density on ungrafted nanoparticles (>30% w/w of total protein), its adsorption is reduced to less than 5% w/w when nanoparticles are grafted with PEG above ~0.5 PEG/nm^2. Together, these findings suggest that PEG minimizes macrophage uptake by selectively suppressing the adsorption of specific serum proteins, not by eliminating serum protein adsorption entirely.

It is unclear what mechanism is responsible for serum-independent macrophage uptake of nanoparticles grafted with PEG at high density. It is possible that a receptor-independent process such as fluid phase pinocytosis contributes, consistent with the observation that intracellular nanoparticles are mostly confined to large (>500 nm) vesicles when grafted with PEG at

dx.doi.org/10.1021/ja2084338 | J. Am. Chem.Soc. 2012, 134, 2139–2147

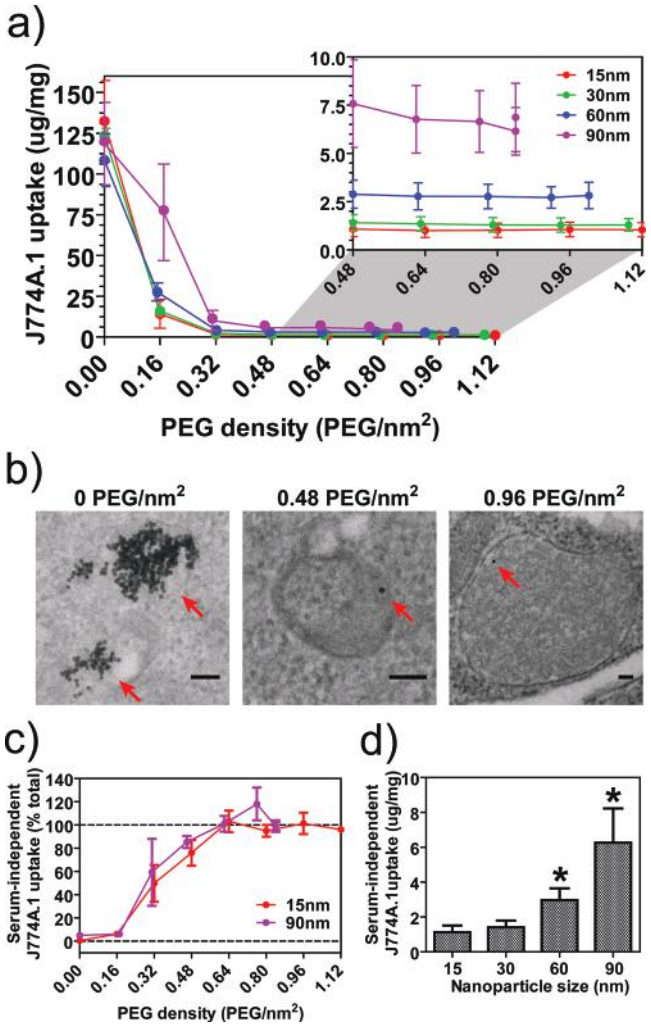

Figure 4. Macrophage uptake depends on nanoparticle size and PEG density. (a) Uptake of PEG-grafted gold nanoparticles by J774A.1 macrophage-like cells. Ungrafted nanoparticles were taken up efficiently, regardless of size. Macrophage uptake decreases rapidly as PEG density increases, but is not eliminated even at the highest PEG densities tested (inset). Gold nanoparticle uptake was measured by ICP-AES after 4 h of incubation with cells. Uptake is reported as ug of gold per mg of total cell protein. (b) Representative TEM micrographs showing subcellular localization of internalized gold nanoparticles grafted with PEG at 0 (ungrafted), 0.48, and 0.96 PEG/nm^2. Ungrafted nanoparticles were observed as aggregated masses in intracellular vesicles, while nanoparticles grafted with PEG were dispersed and present in low numbers in intracellular vesicles. Red arrows indicate nanoparticles. Scale bars represent 100 nm. (c) PEG density determines the mechanism of macrophage uptake. % serum-independent macrophage uptake is J774A.1 uptake (in serum-free media) of nanoparticles blocked with serum albumin relative to nanoparticles preincubated in whole serum. (d) Serum-independent uptake is size-dependent. Reported values are the average total J774A.1 uptake at PEG grafting densities at or above 0.64 PEG/nm^2. Hypothesis testing was performed using the *t* test. *$p < 0.05$ relative to 15 nm. All data points are mean ± SEM from 3–5 independent replicates.

high density (Figure S7).[55−57] Alternatively, uptake may be the result of direct interaction between the PEG chain or distal methoxy group and the cell surface.[40] The lower efficiency of serum-independent macrophage uptake relative to serum-dependent uptake implies that these interactions are considerably weaker than direct protein−receptor interactions. It is unlikely that they are covalent or electrostatic but may instead be weaker hydrophobic interactions or hydrogen bonding.[41] These interactions are not strong enough to support the adsorption of soluble serum proteins, but the avidity of many such interactions over many cell surface proteins, lipids, or macromolecules may be sufficient to drive macrophage uptake.[58,59] As such, reducing or eliminating macrophage uptake of PEG-grafted nanoparticles will require chemically modifying the polymer chain and distal terminal group to reduce direct interactions with the cell surface.[60]

The uptake efficiency of ungrafted nanoparticles showed no statistically significant dependence on nanoparticle size (Figure S9a). This is contrary to some published studies that have reported a maximum cell uptake efficiency for 40−60 nm nanoparticles.[26,27,61] Differences in nanoparticle surface chemistry, cell type, culture protocols, and uptake pathway may account for this disparity.[62] However, equivalent reductions in adsorbed serum protein density by PEG had a more profound effect on macrophage uptake of larger rather than smaller nanoparticles (Figure S9d). At the same time, serum-independent macrophage uptake of larger nanoparticles is more efficient than smaller nanoparticles (Figure 4d). The enhanced avidity of many protein−receptor or PEG−cell interactions on larger nanoparticles can explain both of these observations.[59,63] This may also explain why smaller PEG-grafted nanoparticles tend to have longer blood half-lives than larger nanoparticles, even when they are both grafted with PEG at high density.[37] In summary, while nanoparticle size does not significantly influence the balance between serum-dependent and serum-independent macrophage uptake, it does influence the uptake efficiency of PEG-grafted nanoparticles.

■ CONCLUSIONS

The results of this study are summarized schematically in Figure 5. PEG grafting density controls the adsorption of over 70 different serum proteins to gold nanoparticles. Increasing PEG density decreases total serum protein adsorption, and also changes the composition of the adsorbed protein layer. Nanoparticle size influences serum protein adsorption by modulating PEG−PEG steric interactions. PEG density and nanoparticle size together determine the mechanism and efficiency of subsequent macrophage uptake, probably by controlling either the identity or accessibility of adsorbed serum proteins. Below ~0.16 PEG/nm^2, macrophage uptake depends on the presence of adsorbed serum proteins (serum-dependent uptake). Above ~0.64 PEG/nm^2, macrophage uptake does not depend on the presence of adsorbed proteins (serum-independent uptake). Serum-dependent macrophage uptake is more efficient than serum-independent uptake, presumably as a result of differences in the strength of nanoparticle−cell interactions. Interestingly, serum-independent uptake was more efficient for the largest nanoparticles tested (90 nm). Ultimately, we have shown that the efficiency and mechanism of nanoparticle uptake by macrophages can be controlled by changing nanoparticle size and PEG grafting density. The extent to which PEG blocks serum protein adsorption at high grafting density shows that it is an effective strategy to broadly overcome nonspecific serum-dependent cell uptake of nanomaterials. However, even at high density, PEG cannot completely eliminate cell uptake. Elucidating the mechanism of macrophage uptake of PEG-grafted nanomaterials will be a

dx.doi.org/10.1021/ja2084338 | J. Am. Chem.Soc. 2012, 134, 2139−2147

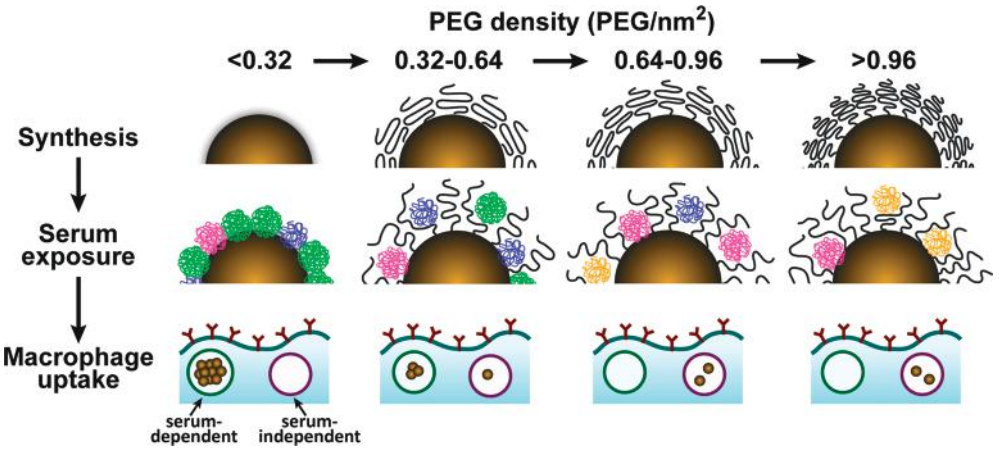

Figure 5. Schematic illustrating the influence of PEG density on serum protein adsorption to gold nanoparticles and their subsequent uptake by macrophages. The top panel shows as-synthesized gold nanoparticles grafted with PEG at increasing density. As PEG density increases, PEG volume decreases as a result of PEG–PEG steric interactions. The middle panel illustrates how PEG density determines the amount and relative abundance of serum proteins adsorbed to the gold nanoparticle surface after serum exposure. At low PEG densities (<0.32 PEG/nm^2), proteins from cluster A (green) adsorb preferentially. At low-intermediate PEG densities (0.32–0.64 PEG/nm^2), proteins from cluster B (blue) adsorb preferentially. At intermediate-high PEG densities (0.64–0.96 PEG/nm^2), proteins from cluster C (fuchsia) adsorb preferentially. At high PEG densities (>0.96 PEG/nm^2), proteins from cluster D (orange) adsorb preferentially. The lower panel shows that at low PEG densities, macrophage uptake is efficient and serum-dependent. At high PEG densities, macrophage uptake is driven predominantly by a less efficient serum-independent mechanism. Structures in this diagram are conceptualized for illustrative purposes.

valuable resource for designing alternative formulations with improved performance.

EXPERIMENTAL PROCEDURES

Materials. All materials were used as received, unless otherwise indicated. Water was filtered using a Nanopure system prior to use (Thermo-Fisher Scientific). All stock solutions were prepared in water, unless otherwise indicated. All chemicals are from Sigma-Aldrich, unless otherwise indicated.

Cell Culture. J774A.1 (American Type Tissue Culture) cells were maintained in 10 cm tissue culture dishes (BD Biosciences) and growth media consisting of RPMI 1640 supplemented with 10% v/v fetal bovine serum (FBS) and 1% v/v penicillin–streptomycin at 37 °C with 5% CO_2.

Gold Nanoparticle Synthesis. Gold nanoparticles ranging in size from 15 to 90 nm were synthesized by citrate reduction and seed-mediated growth.[39] To make 15 nm nanoparticles, 100 mL of 0.25 mM $HAuCl_4$ was brought to a boil in a 250 mL Erlenmeyer flask containing a 1.5 in. magnetic stir-bar. Next, 1 mL 3% w/v sodium citrate was added under rapid stirring. The solution color changed from clear to purple to bright red over the course of ∼5 min. Boiling and stirring were continued for 10 min. The solution was then cooled on ice and diluted to 100 mL with water.

The 30, 60, and 90 nm gold nanoparticles were synthesized by surface-assisted reduction of ionic gold by hydroquinone.[39] Water was added to a 250 mL Erlenmeyer flask containing a magnetic stir-bar, followed by 15 mM sodium citrate, 25 mM $HAuCl_4$, and 15 nm gold nanoparticles. The volume of each solution depended on the desired nanoparticle size (Table S1). Mixtures were either maintained at room temperature (60/90 nm) or cooled to 4 °C (30 nm). Under rapid stirring, 25 mM hydroquinone was added to each flask (Table S1). Flasks were stirred overnight at room temperature to complete the reduction of ionic gold and particle growth.

After synthesis, absorbance spectra of aqueous suspensions of gold nanoparticles were recorded from 350 to 900 nm on a UV-1601PC UV–visible spectrophotometer (Shimadzu) to confirm the presence of a single narrow localized surface plasmon resonance peak, without a long-wavelength shoulder characteristic of aggregates.[62] The plasmon peak was centered at ∼518 nm for 15 nm particles, but red-shifted and broadened as nanoparticle size increased.

Poly(ethylene glycol) Grafting. Aliquots of 10, 20, 40, and 60 mL of as-synthesized 15, 30, 60, and 90 nm gold nanoparticles, respectively, were concentrated by centrifugation at 4 °C and combined (see Table S2 for centrifugation speeds) to form stocks with a total surface area of ∼102 cm^2. Concentrated stocks were washed three times in 750 μL of 0.25 mM sodium citrate/0.05% v/v TWEEN20 by centrifugation. Here, TWEEN20 was used to solubilize surface-adsorbed hydroquinone and maintain colloidal stability during washing. Particles were then concentrated and resuspended in 90 μL of H_2O and added to 10 μL of mPEG5K-SH (NOF Sunbright). For each nanoparticle size, PEG stock concentrations of 0, 0.27, 0.54, 0.83, 1.08, 1.36, 1.63, 1.90, and 16.9 mM were used to give average grafting stoichiometries (ρ_{graft}) of 0, 0.16, 0.32, 0.48, 0.64, 0.80, 1.12, and 10 PEG/nm^2, respectively. PEG coordination to the gold surface was completed by incubation in a water bath at 60 °C for 1 h. After incubation, PEG-grafted nanoparticles were pelleted by centrifugation. The free thiol concentration in the supernatant ($[SH]_{sn}$) was measured by reduction of 5,5′-dithiobis(2-nitrobenzoic acid) (Pierce). Coordination efficiency (θ) is calculated from the formula $\theta = 1 - [SH]_{sn}/[SH]_{total}$, where $[SH]_{total}$ is the thiol concentration in a particle-free control sample containing an equal concentration of mPEG5K-SH. PEG grafting density (ρ_{PEG}) was determined by multiplying the coordination efficiency by the grafting stoichiometry: $\rho_{graft} = \theta\rho_{graft}$. PEG-grafted nanoparticles were washed twice in 750 μL of 0.25 mM sodium citrate/0.05% v/v TWEEN20 to remove unbound PEG and resuspended in 40 μL of water to make PEG-grafted gold nanoparticle stock solutions.

Transmission Electron Microscopy (TEM). Aliquots of 1 μL of PEG-grafted gold nanoparticle stock solutions were diluted to 5 μL with water and deposited on Formvar-coated copper grids (Ted Pella). After 5 min, excess liquid was wicked away, and the remaining thin solution film was allowed to dry. Grids were imaged using an HD2000 STEM (Hitachi) with an accelerating voltage of 200 V to enhance the contrast of the electron-dense gold. Enough frames were collected to capture at least 100 particles per replicate. Nanoparticle size (d) was estimated using the formula $d = 2(A/\pi)^{1/2}$, where A is the cross-sectional area of a particle measured using ImageJ.

Dynamic Light Scattering (DLS). Aliquots of 1 μL of PEG-grafted gold nanoparticle stock solutions were serially diluted in 500 μL of 0.25 mM sodium citrate and transferred to 2.0 mL polystyrene cuvettes. The Z-average hydrodynamic diameter (HD) and polydispersity index (PDI) were measured using a ZetaSizer Nano ZS

dx.doi.org/10.1021/ja2084338 | J. Am. Chem.Soc. 2012, 134, 2139–2147

(Malvern Instruments) with attenuator position set to 4.65 mm. Nanoparticle dilutions that gave an attenuator setting of between 6 and 9 were used for measurement. The hydrodynamic volume per PEG molecule V_{PEG} on a gold nanoparticle of radius R (in nm) was calculated using the formula $V_{PEG} = (V_\rho - V_0)/(4\pi R^2_\rho)$, where V_ρ is the hydrodynamic volume of a gold nanoparticle grafted with PEG at a density ρ. V_ρ is calculated using the formula $V_\rho = \pi D_\rho^3/6$, where D_ρ is the hydrodynamic diameter of a gold nanoparticle grafted with PEG at a density ρ.

Serum Protein Adsorption and Purification. Aliquots of 20 μL of each PEG-grafted gold nanoparticle stock solution (a total surface area of 51 cm^2) were rapidly added to 500 μL of 10% v/v human serum diluted in phosphate-buffered saline (PBS) containing 5 mM ethylenediaminetetraacetic acid (EDTA). None of the preparations showed visible signs of aggregation. Particles were incubated with serum for 2 h at room temperature to allow protein adsorption. Particles were then washed to remove unbound serum by three rounds of centrifugation (18000*g* for 30 min at 4 °C) and resuspension in 750 μL of PBS containing 5 mM EDTA and 0.05% v/v TWEEN20. Here, TWEEN20 is used to prevent agglomeration of nanoparticles during centrifugation. As a control for nonspecific protein adsorption, equal volumes of serum without particles were treated in parallel. After washing, particles were pelleted by centrifugation, and the supernatant was discarded, leaving a pellet volume of ~15 μL. Next, 8 μL of 4× LDS sample buffer (Invitrogen) and 4 μL of 500 mM dithiothreitol (DTT) was added to the pellets, followed by incubation at 70 °C for 1 h to release adsorbed proteins. Particles aggregated during this treatment and were centrifuged at 18000*g* for 15 min to form a tight pellet. Supernatants containing isolated protein (~30 μL) were transferred to a new tube. A 6.5 μL aliquot of each sample was reserved for PAGE. The remaining protein was precipitated by adding 950 μL of 10% w/v trichloroacetic acid (TCA) in acetone followed by overnight incubation at −80 °C. Precipitates were pelleted by centrifugation (18000*g* for 15 min at 4 °C) and the supernatant discarded. The pellet was dissolved in 500 μL of 0.03% w/v sodium deoxycholate and precipitated by adding 100 μL of 72% w/v TCA followed by incubation for 30 min on ice. The resulting precipitate was pelleted by centrifugation (18000*g* for 15 min at 4 °C) and the supernatant discarded. The pellet was washed once in 1 mL acetone at −30 °C, and dried in a fume hood. After this treatment, the protein pellet is free of salts, PEG, reducing agents, and detergent. Pellets were then dissolved in 50 μL of 50 mM ammonium bicarbonate containing 0.1% w/v Rapigest (Waters). Rapigest was added to aid solubilization and subsequent trypsin digestion.

Bicinchoninic Acid (BCA) Assay. Aliquots of 10 μL of protein isolates were diluted with 40 μL of 2% w/v sodium dodecyl sulfate and transferred to a 96-well plate, along with 50 μL aliquots of a bovine serum albumin (BSA) (Pierce) serial dilution. Next, 200 μL of freshly prepared BCA working reagent (Pierce) was added to each well, and the plate was incubated at 37 °C for 30 min or until color was sufficiently developed. Absorbance at 562 nm was measured using a plate reader (Tecan Sunrise). The absorbance of the particle-free control was subtracted from the samples and total protein concentration calculated relative to the BSA standard.

Polyacrylamide Gel Electrophoresis (PAGE) and Densitometry. Aliquots of 6.5 μL of isolated serum protein were mixed with 2.5 μL of 4× LDS sample buffer (Invitrogen) and 1 μL of 500 mM DTT and incubated at 70 °C for 30 min. Protein aliquots, along with 2 μL of Benchmark molecular weight ladder (Invitrogen), were loaded on a 4−12% Bis-Tris gel in MOPS running buffer (Invitrogen) and resolved at 200 V for 55 min at 4 °C. After electrophoresis, gels were fixed with 10% v/v acetic acid in 40% v/v ethanol overnight and stained with Krypton fluorescent protein stain (Pierce) according to the manufacturer's protocol. Stained gels were scanned on a Typhoon laser scanner (Amersham) with excitation/emission set to 532/580 nm, photomultiplier tube accelerating voltage set to 500 V, and pixel size set to 50 μm. Scanned images were imported in ImageJ, background-subtracted, and cropped. Lane and molecular weight labels were added in Adobe Illustrator. Band intensity and net lane intensity was quantified by densitometry in ImageJ and analyzed using Matlab.

Liquid Chromatography Tandem Mass Spectrometry (LC-MS/MS). A 15 μL portion of isolated serum protein from 15 nm gold nanoparticles grafted with PEG at varying density was mixed with 1 μL of 100 mM dithiothreitol (Sigma) and incubated at 37 °C for 60 min. Next, 1 μL of 500 mM iodoacetamide was added and the solution incubated for 60 min in the dark at room temperature to alkylate cysteines. Finally, 1 μg of proteomics grade trypsin was added to each sample, followed by overnight digestion at 37 °C. Digestion was halted and Rapigest detergent cleaved by adding formic acid to 10% v/v, followed by incubation at 37 °C for 30 min. Precipitates were cleared by centrifugation at 18000*g* for 15 min.

In the next step, 9 μL of digested protein was injected into a reverse phase microcapillary liquid chromatography column for separation using the EASY-nLC system (Proxeon). The microcapillary chromatography analytical column was constructed in a 100-mm × 75-μm silica capillary tip pulled with a column puller (Sutter Instrument) and packed with 3-μm Luna C18 stationary phase (Phenomenex). The organic gradient was driven by the EASY-nLC system over 105 min using buffers A and B (98% buffer A (95% water, 5% acetonitrile, and 0.1% formic acid) to 90% buffer B (95% acetonitrile and 0.1% formic acid in water) over 45 min) at a flow rate of 300 nL/min. The gradient was held at 2% B for 1 min, followed by a 2-min increase to 6% B, 76-min increase to 26% B, 5-min increase to 90% B, 5-min hold at 90% B, 1-min decrease to 2% B, and 8-min hold at 2% B. Eluted peptides were directly sprayed into an Orbitrap Velos mass spectrometer (Thermo-Fisher Scientific) with collision-activated dissociation using a nanospray ion source (Proxeon). A spray voltage of +2.5 kV was applied. Ten MS/MS data-dependent scans were acquired simultaneously with one high-resolution (60 000) full-scan mass spectrum to provide the amino acid sequence information and mass-to-charge ratio for selected peptide ions. The dynamic exclusion list was enabled to exclude a maximum of 500 ions for 30 s. A 30-min wash step was applied after each sample to reduce cross-contamination.

Analysis of LC-MS/MS Spectra. RAW files were extracted from the mass spectrometry data with the ReAdW program and submitted to database search using SEQUEST v2.7 and a UniProt/SwissProt protein database FASTA file containing 22,491 human proteins as well as a reversed sequence decoy protein set to determine false discovery rate (FDR).[64] Search parameters were set to allow for one missed cleavage site and one fixed modification of +57 for cysteine using precursor tolerance of 3 m/z. Matched peptides were further filtered at the precursor ion spectra level using a 20 ppm cutoff. Protein hits were filtered using the StatQuest[65] program with a confidence level of 99%. The resulting peptide identification false discovery rate was 2.02%.

The database search identified 147 unique proteins, excluding keratins and proteins identified in only a single experimental replicate. Some identified proteins may be false positives, as a result of contamination during sample preparation or analysis. The relative abundance (by mass) of the identified proteins was estimated by the formula: $wt\%_A = SpC_A/SpC_{tot}$, where SpC_A is the number of spectral counts of a protein A at a given PEG density, and SpC_{tot} is the total spectral counts for all adsorbed proteins at that same PEG density.[50] Average spectral counts for each identified protein from three independent experimental replicates are reported in Table S3. A heat map showing the weight fractions of the adsorbed proteins was generated using the Matlab function "clustergram". Only proteins with $wt\%_A > 0.25\%$ are reported in the heat map (70 total). The intensity of the yellow color is related to the average weight fraction by a shifted sigmoid function.

Cluster Analysis. Identified proteins were clustered into groups based on correlation in their relative abundance. Pearson correlation coefficients were used and programmed in Matlab. The unweighted average distance (UPGMA) was used to compute distances between clusters. Groups containing fewer than three proteins were excluded. Out of 70 analyzed proteins, 64 clustered into one of four groups labeled A, B, C, or D. Weight fractions of each protein within the four

groups were added together to give the total weight fraction for the group.

J774A.1 Uptake and Transmission Electron Microscopy (TEM). J774A.1 cells were harvested from ~80% confluent tissue culture dishes using a cell scraper and adjusted to a concentration of 1.2×10^6 cells/mL in growth media. Next, 1 mL of the cell suspension was transferred to each well of a 6-well tissue culture plate (BD Biosciences) and grown to ~90% confluence. Aliquots of 12, 6, 3, and 2 μL of 15, 30, 60, and 90 nm PEG-grafted gold nanoparticle stock solutions were incubated in 400 μL of 10% v/v human serum (diluted in PBS containing 5 mM EDTA) for 2 h at room temperature. Particles were pelleted and resuspended in 1.5 mL growth media to prepare for cell culture. Growth media was aspirated from the cells and replaced with 1.5 mL of media containing nanoparticles. Particle aliquots were adjusted such that each well contained a total of 148 μg of gold, regardless of nanoparticle size. Cells were incubated with particles for 4 h at 37 °C. This time period was long enough to allow sufficient cell uptake, but short enough to limit sedimentation of larger nanoparticles.[66] After incubation, media containing nanoparticles was aspirated and discarded. Cells were washed three times with 3 mL PBS to remove nanoparticles that are free in solution or loosely adhered to the cell surface.[62,67,68] Residual PBS was aspirated. Cells were collected in a microcentrifuge tube. A 5 μL aliquot was transferred to fixative, stained, sliced, and imaged by TEM. Remaining cells were lysed by adding 1 mL of 2% sodium dodecyl sulfate to each well followed by incubation for 1 h at 37 °C. 1 mL of cell lysate was transferred to a microcentrifuge tube and sonicated with a probe sonicator (Misonix) to break apart cellular debris. Total cell protein was measured by the BCA assay relative to a BSA standard (Pierce). Average protein content per cell was measured as ~180 pg/cell.

Inductively Coupled Plasma Atomic Emission Spectroscopy (ICP-AES). Aliquots of 400 μL of sonicated cell lysates were diluted with 3.6 mL water in a 15 mL conical tube (BD Biosciences). Gold content in the lysates was measured relative to a serial dilution of gold standard (High Purity Standards) using ICP-AES (Perkin-Elmer). Total J774A.1 uptake was normalized for cell number by dividing total gold concentration by total cell protein, and reported as micrograms of gold per milligram of cell protein.

Serum-Free J774A.1 Uptake. Aliquots of 12, 6, 3, and 2 μL of 15, 30, 60, and 90 nm PEG-grafted gold nanoparticle stock solutions were added to 10% v/v human serum and incubated at room temperature for 1 h. Particles were then pelleted and resuspended in 500 μL of RPMI 1640 containing 10% FBS. As a control, 12, 6, 3, and 2 μL aliquots of the same 15, 30, 60, and 90 nm PEG-grafted gold nanoparticles were added to 5 mg/mL BSA in PBS. Both the samples and controls were incubated for 2 h at 37 °C. Particles incubated in BSA only were transferred to 0.5 mg/mL mPEG5K-SH (NOF Sunbright) for 10 min to block any exposed gold surface. Both sets of particles were washed into 1.5 mL RPMI containing 5 mg/mL BSA to prepare for cell culture. J774A.1 cells were plated in 6-well plates and grown to ~90% confluence in growth media as described above. Cells were washed once with 3 mL of PBS to remove residual FBS. PBS was aspirated and replaced with media containing gold nanoparticles. Cells were incubated with particles for 4 h at 37 °C. Total nanoparticle uptake of both serum-treated (U_{ser}), and BSA-treated (U_{BSA}) nanoparticles was measured using ICP-AES as described above. The fraction of total cell uptake that is serum-independent (F_{ind}) was calculated using the formula $F_{ind} = (U_{BSA}/U_{FBS})$.

Statistics. Statistical analysis was performed using Matlab. The distribution of observations between experimental replicates was assumed to be normal. The t test was used for hypothesis testing. Linear regression was performed by minimization of the sum of squares. Correlation between sets of variables was performed using Pearson correlation coefficients.

■ ASSOCIATED CONTENT

Ⓢ Supporting Information

Supplementary Figures S1−S9 and Tables S1−S3. This material is available free of charge via the Internet at http://pubs.acs.org.

■ AUTHOR INFORMATION

Corresponding Author

warren.chan@utoronto.ca

■ ACKNOWLEDGMENTS

This work was supported by grants from the Canadian Institute of Health Research (MOP-93532), Canadian Research Chair Fellowship (950-203-403), Natural Sciences and Engineering Research Council (NETGP 35015-07 and RGPIN 288231-09), Canadian Foundation for Innovation, and Ministry of Research and Innovation. C.D.W. acknowledges NSERC for a graduate fellowship.

■ REFERENCES

(1) Choi, C. L.; Alivisatos, A. P. *Annu. Rev. Phys. Chem.* **2010**, *61*, 369.
(2) Xia, D.; Ku, Z.; Lee, S. C.; Brueck, S. R. J. *Adv. Mater.* **2011**, *23*, 147.
(3) Nie, S.; Xing, Y.; Kim, G. J.; Simons, J. W. *Annu. Rev. Biomed. Eng.* **2007**, *9*, 257.
(4) Mamo, T.; Moseman, E. A.; Kolishetti, N.; Salvador-Morales, C.; Shi, J.; Kuritzkes, D. R.; Langer, R.; Andrian, U. V.; Farokhzad, O. C. *Nanomedicine* **2010**, *5*, 269.
(5) Lobatto, M. E.; Fuster, V.; Fayad, Z. A.; Mulder, W. J. M. *Nat. Rev. Drug Discovery* **2011**, *10*, 835.
(6) McCarthy, J. R.; Korngold, E.; Weissleder, R.; Jaffer, F. A. *Small* **2010**, *6*, 2041.
(7) Nie, S. *Nanomedicine* **2010**, *5*, 523.
(8) Li, S. D.; Huang, L. *Mol. Pharmaceutics* **2008**, *5*, 496.
(9) Sanhai, W. R.; Sakamoto, J. H.; Canady, R.; Ferrari, M. *Nat. Nanotechnol.* **2008**, *3*, 242.
(10) Ballou, B.; Lagerholm, B. C.; Ernst, L. A.; Bruchez, M. P.; Waggoner, A. S. *Bioconjugate Chem.* **2004**, *15*, 79.
(11) Owens, D. E. III; Peppas, N. A. *Int. J. Pharm.* **2006**, *307*, 93.
(12) Fischer, H. C.; Liu, L.; Pang, K. S.; Chan, W. C. W. *Adv. Funct. Mater.* **2006**, *16*, 1299.
(13) Moghimi, S. M.; Hunter, A. C.; Murray, J. C. *Pharmacol. Rev.* **2001**, *53*, 283.
(14) Fischer, H. C.; Hauck, T. S.; Gómez-Aristizábal, A.; Chan, W. C. W. *Adv. Mater.* **2010**, *22*, 2520.
(15) Allen, T. M. *Adv. Drug Delivery Rev.* **1988**, *2*, 55.
(16) Derfus, A. M.; Chan, W. C. W.; Bhatia, S. N. *Nano Lett.* **2004**, *4*, 11.
(17) Yang, R. S. H.; Chang, L. W.; Wu, J. P.; Tsai, M. H.; Wang, H. J.; Kuo, Y. C.; Yeh, T. K.; Yang, C. S.; Lin, P. *Environ. Health Perspect.* **2007**, *115*, 1339.
(18) Hauck, T. S.; Anderson, R. E.; Fischer, H. C.; Newbigging, S.; Chan, W. C. W. *Small* **2010**, *6*, 138.
(19) Murday, J. S.; Siegel, R. W.; Stein, J.; Wright, J. F. *Nanomed. Nanotechnol. Biol. Med.* **2009**, *5*, 251.
(20) Cedervall, T.; Lynch, I.; Lindman, S.; Berggård, T.; Thulin, E.; Nilsson, H.; Dawson, K. A.; Linse, S. *Proc. Natl. Acad. Sci. U.S.A.* **2007**, *104*, 2050.
(21) Walkey, C. D.; Chan, W. C. W. *Chem. Soc. Rev.* **2012**, DOI: 10.1039/C1CS15233E.
(22) Nel, A. E.; Mädler, L.; Velegol, D.; Xia, T.; Hoek, E. M. V.; Somasundaran, P.; Klaessig, F.; Castranova, V.; Thompson, M. *Nat. Mater.* **2009**, *8*, 543.
(23) Anderson, N. L.; Polanski, M.; Pieper, R.; Gatlin, T.; Tirumalai, R. S.; Conrads, T. P.; Veenstra, T. D.; Adkins, J. N.; Pounds, J. G.; Fagan, R.; Lobley, A. *Mol. Cell. Proteomics* **2004**, *3*, 311.

(24) Deng, Z. J.; Liang, M.; Monteiro, M.; Toth, I.; Minchin, R. F. *Nat. Nanotechnol.* **2011**, *6*, 39.
(25) Moghimi, S. M.; Andersen, A. J.; Hashemi, S. H.; Lettiero, B.; Ahmadvand, D.; Hunter, A. C.; Andresen, T. L.; Hamad, I.; Szebeni, J. *J. Controlled Release* **2010**, *146*, 175.
(26) Chithrani, B. D.; Ghazani, A. A.; Chan, W. C. W. *Nano Lett.* **2006**, *6*, 662.
(27) Zhang, S.; Li, J.; Lykotrafitis, G.; Bao, G.; Suresh, S. *Adv. Mater.* **2009**, *21*, 419.
(28) Davis, M. E.; Chen, Z.; Shin, D. M. *Nat. Rev. Drug Discovery* **2008**, *7*, 771.
(29) Lundqvist, M.; Stigler, J.; Elia, G.; Lynch, I.; Cedervall, T.; Dawson, K. A. *Proc. Natl. Acad. Sci. U.S.A.* **2008**, *105*, 14265.
(30) Vonarbourg, A.; Passirani, C.; Saulnier, P.; Benoit, J. P. *Biomaterials* **2006**, *27*, 4356.
(31) Satulovsky, J.; Carignano, M. A.; Szleifer, I. *Proc. Natl. Acad. Sci. U.S.A.* **2000**, *97*, 9037.
(32) Jeon, S. I.; Lee, J. H.; Andrade, J. D.; De Gennes, P. G. *J. Colloid Interface Sci.* **1991**, *142*, 149.
(33) Szleifer, I. *Biophys. J.* **1997**, *72*, 595.
(34) Paciotti, G. F.; Myer, L.; Weinreich, D.; Goia, D.; Pavel, N.; McLaughlin, R. E.; Tamarkin, L. *Drug Delivery* **2004**, *11*, 169.
(35) Niidome, T.; Yamagata, M.; Okamoto, Y.; Akiyama, Y.; Takahashi, H.; Kawano, T.; Katayama, Y.; Niidome, Y. *J. Controlled Release* **2006**, *114*, 343.
(36) Park, K. *J. Controlled Release* **2010**, *142*, 147.
(37) Perrault, S. D.; Walkey, C.; Jennings, T.; Fischer, H. C.; Chan, W. C. W. *Nano Lett.* **2009**, *9*, 1909.
(38) Li, S. D.; Huang, L. *Biochim. Biophys. Acta, Biomembr.* **2009**, *1788*, 2259.
(39) Perrault, S. D.; Chan, W. C. W. *J. Am. Chem. Soc.* **2009**, *131*, 17042.
(40) Unsworth, L. D.; Sheardown, H.; Brash, J. L. *Langmuir* **2008**, *24*, 1924.
(41) Unsworth, L. D.; Sheardown, H.; Brash, J. L. *Langmuir* **2005**, *21*, 1036.
(42) Pasche, S.; De Paul, S. M.; Vörös, J.; Spencer, N. D.; Textor, M. *Langmuir* **2003**, *19*, 9216.
(43) Zhu, X. Y.; Jun, Y.; Staarup, D. R.; Major, R. C.; Danielson, S.; Boiadjiev, V.; Gladfelter, W. L.; Bunker, B. C.; Guo, A. *Langmuir* **2001**, *17*, 7798.
(44) Kingshott, P.; Thissen, H.; Griesser, H. J. *Biomaterials* **2002**, *23*, 2043.
(45) Harder, P.; Grunze, M.; Dahint, R.; Whitesides, G. M.; Laibinis, P. E. *J. Phys. Chem. B* **1998**, *102*, 426.
(46) Tsukanova, V.; Salesse, C. *J. Phys. Chem. B* **2004**, *108*, 10754.
(47) Hill, H. D.; Millstone, J. E.; Banholzer, M. J.; Mirkin, C. A. *ACS Nano* **2009**, *3*, 418.
(48) Dobrovolskaia, M. A.; Patri, A. K.; Zheng, J.; Clogston, J. D.; Ayub, N.; Aggarwal, P.; Neun, B. W.; Hall, J. B.; McNeil, S. E. *Nanomed. Nanotechnol. Biol. Med.* **2009**, *5*, 106.
(49) Bousette, N.; Kislinger, T.; Fong, V.; Isserlin, R.; Hewel, J. A.; Emili, A.; Gramolini, A. O. *J. Proteome Res.* **2009**, *8*, 1887.
(50) Griffin, N. M.; Yu, J.; Long, F.; Oh, P.; Shore, S.; Li, Y.; Koziol, J. A.; Schnitzer, J. E. *Nat. Biotechnol.* **2010**, *28*, 83.
(51) Jeon, S. I.; Andrade, J. D. *J. Colloid Interface Sci.* **1991**, *142*, 159.
(52) Soma, C. E.; Dubernet, C.; Barratt, G.; Benita, S.; Couvreur, P. *J. Controlled Release* **2000**, *68*, 283.
(53) van Lookeren Campagne, M.; Wiesmann, C.; Brown, E. J. *Cell. Microbiol.* **2007**, *9*, 2095.
(54) Mosqueira, V. C. F.; Legrand, P.; Gulik, A.; Bourdon, O.; Gref, R.; Labarre, D.; Barratt, G. *Biomaterials* **2001**, *22*, 2967.
(55) Buono, C.; Anzinger, J. J.; Amar, M.; Kruth, H. S. *J. Clin. Invest.* **2009**, *119*, 1373.
(56) Brandenberger, C.; Mühlfeld, C.; Ali, Z.; Lenz, A. G.; Schmid, O.; Parak, W. J.; Gehr, P.; Rothen-Rutishauser, B. *Small* **2010**, *6*, 1669.
(57) Bartneck, M.; Keul, H. A.; Singh, S.; Czaja, K.; Bornemann, J.; Bockstaller, M.; Moeller, M.; Zwadlo-Klarwasser, G.; Groll, J. *ACS Nano* **2010**, *4*, 3073.
(58) Calson, C. B.; Mowery, P.; Owen, R. M.; Dykhuizen, E. C.; Kiessling, L. L. *ACS Chem. Biol.* **2007**, *2*, 119.
(59) Hong, S.; Leroueil, P. R.; Majoros, I. J.; Orr, B. G.; Baker, J. R. Jr.; Banaszak Holl, M. M. *Chem. Biol.* **2007**, *14*, 107.
(60) Statz, A. R.; Meagher, R. J.; Barron, A. E.; Messersmith, P. B. *J. Am. Chem. Soc.* **2005**, *127*, 7972.
(61) Lu, F.; Wu, S. H.; Hung, Y.; Mou, C. Y. *Small* **2009**, *5*, 1408.
(62) Albanese, A.; Chan, W. C. W. *ACS Nano* **2011**, *5*, 5478.
(63) Jiang, W.; Kim, B. Y. S.; Rutka, J. T.; Chan, W. C. W. *Nat. Nanotechnol.* **2008**, *3*, 145.
(64) Elias, J. E.; Gygi, S. P. *Nat. Methods* **2007**, *4*, 207.
(65) Kislinger, T.; Rahman, K.; Radulovic, D.; Cox, B.; Rossant, J.; Emili, A. *Mol. Cell. Proteomics* **2003**, *2*, 96.
(66) Cho, E. C.; Zhang, Q.; Xia, Y. *Nat. Nanotechnol.* **2011**, *6*, 385.
(67) Cho, E. C.; Xie, J.; Wurm, P. A.; Xia, Y. *Nano Lett.* **2009**, *9*, 1080.
(68) dos Santos, T.; Varela, J.; Lynch, I.; Salvati, A.; Dawson, K. A. *Small* **2011**, *7*, 3341.